Cytoskeleton-extracellular matrix interaction is required to maintain mitochondrial Ca^{2+} control in mouse skeletal muscle fibres.

Authors

Charlotte Gineste[a,d], Sara Henriksson[b], Andrés Hernández[a,e], Arthur J. Cheng[a,f], Thomas Chaillou[a,g], Sabine U. Vorrink[a], Sonia Youhanna[a], Andreas Buttgereit[c], Dominik Schneidereit[c], Oliver Friedrich[c], Kjell Hultenby[c], Joseph D. Bruton[a], Niklas Ivarsson[a], Linda Sandblad[b], Volker M. Lauschke[a]* and Håkan Westerblad[a]*

[a] Department of Physiology and Pharmacology, Karolinska Institutet, 171 77 Stockholm, Sweden

[b] Umeå Core Facility for Electron Microscopy, Department of Chemistry, Umeå University, 901 87 Umeå, Sweden

[c] Institute of Medical Biotechnology, Department of Chemical and Biological Engineering, Friedrich-Alexander University of Erlangen-Nürnberg, 91052 Erlangen, Germany

[c] Department of Laboratory Medicine, Karolinska Institutet, Karolinska University Hospital Huddinge, 141 86 Huddinge, Sweden

[d] Present address: Institut de Génétique et de Biologie Moléculaire et Cellulaire (IGBMC), Illkirch, France

[e] Present address: University of California Merced, Merced, CA 95340, USA

[f] Present address: School of Kinesiology and Health Sciences, York University, M3J 1P3 Toronto, Canada

[g] Present address: Örebro University, 701 82 Örebro, Sweden

*Shared corresponding authors. Address as above.

E-mail: hakan.westerblad@ki.se; Volker.lauschke@ki.se;

Telephone: +46 8 524 872 53

Short title: Cell-matrix control of mitochondrial Ca^{2+}

Summary

Cells rapidly lose their physiological phenotype upon isolation from their native microenvironment. Here, we investigated the role of the extracellular matrix (ECM) for mitochondrial morphology and Ca^{2+} handling in adult mouse skeletal muscle fibres. Adult skeletal muscle fibres were isolated from mouse toe muscle either by collagenase-induced dissociation of the ECM or by mechanical dissection that leaves the proximate ECM intact. Experiments were generally performed four hours after cell isolation. At this time, the expression of genes encoding for structural proteins was lower in enzymatically dissociated than in mechanically dissected fibres. Mitochondrial appearance was grossly similar in the two groups, but 3D electron microscopy revealed shorter and less branched mitochondria in enzymatically dissociated than in mechanically dissected fibres. The increase in free cytosolic [Ca^{2+}] during repeated tetanic stimulation was similar in the two groups of fibres, but this was accompanied by an excessive mitochondrial Ca^{2+} uptake only in enzymatically dissociated muscle fibres. The aberrant mitochondrial Ca^{2+} uptake was partially prevented by the mitochondrial Ca^{2+} uniporter inhibitor Ru360 and by cyclosporine A and NV556, which inhibit the mitochondrial matrix protein PPIF (also called cyclophilin D). Importantly, inhibition of PPIF with NV556 significantly improved survival of mice with mitochondrial myopathy in which muscle mitochondria take up excessive amounts of Ca^{2+} also with intact ECM. In conclusion, skeletal muscle fibres isolated by collagenase-induced dissociation of the ECM display aberrant mitochondrial Ca^{2+} uptake, which involves a PPIF-dependent mitochondrial Ca^{2+} influx resembling that observed in mitochondrial myopathies.

Key words

Calcium, enzymatic dissociation, extracellular matrix, mitochondria, skeletal muscle fibre

Main

The intracellular secondary messenger Ca^{2+} is of critical importance for a plethora of cellular functions. Within the cell, Ca^{2+} levels are highly compartmentalized and can differ by orders of magnitude between the cytosol and cellular organelles, such as the endo/sarcoplasmic reticulum. Dysregulation of intracellular Ca^{2+} handling is associated with a range of human pathologies, including diabetes [1, 2], neurodegenerative disease [3], cardiac failure [4], and chronic inflammatory conditions [5, 6]. In this context, mitochondrial Ca^{2+} levels have received increasing attention in recent years for their important roles in energy homeostasis, oxidative stress, and apoptosis [7]. A limited and transient increase in free mitochondrial matrix [Ca^{2+}] ($[Ca^{2+}]_{mit}$) can stimulate mitochondrial respiration and hence play an integral role in the regulation of cellular metabolism, whereas prolonged and excessive uptake can activate apoptotic and necrotic cell signalling pathways [8-10]. Tightly controlled mitochondrial Ca^{2+} entry seems particularly important in skeletal and cardiac muscle cells where contractions are triggered by increases in cytosolic free [Ca^{2+}] ($[Ca^{2+}]_{cyt}$) up to the µM range, and even higher in the vicinity of sarcoplasmic reticulum (SR) Ca^{2+} release sites [11].

A recently identified mitochondrial inner membrane channel, the mitochondrial Ca^{2+} uniporter (MCU), was shown to be a main effector of Ca^{2+} entry [12, 13]. The MCU exists in a protein complex together with several regulators [14], foreshadowing the importance of a tightly controlled Ca^{2+} influx via this channel. However, the presence of mitochondrial Ca^{2+} uptake in cells where the MCU has been genetically ablated illustrates that there are additional mechanisms for mitochondrial Ca^{2+} entry [15, 16]. In contrast to mitochondrial Ca^{2+} uptake, the molecular machinery involved in Ca^{2+} extrusion from mitochondria into the cytosol is tissue specific. In skeletal and cardiac muscles, Ca^{2+} is predominantly exported via the Na^{+}/Ca^{2+} antiporter (NCLX) [17].

Integrin-mediated cell adhesions provide dynamic links between the extracellular matrix (ECM) and the intracellular cytoskeleton [18]. Interactions between the ECM and the cytoskeleton have key roles in the bidirectional mechanical and biochemical signalling between the extracellular environment and the cell interior as well as in the control of cell structure, including the morphology and function of mitochondria [19, 20]. In skeletal muscle fibres, mitochondria are tethered to the SR at sites of Ca^{2+} release [21], and this spatial organization is required for appropriate Ca^{2+} handling [22]. Disturbance of the physical interaction between mitochondria and the endo/sarcoplasmic reticulum in muscle cells can result in altered Ca^{2+} exchange between the two organelles and functional impairment such as impaired insulin sensitivity [23].

It is well-established that the structural linkage between the ECM and the cytoskeleton has a crucial role in the control of gene expression in skeletal muscle fibres, and defects in this linkage underlie the disease progression in several muscular dystrophies [24, 25]. Importantly, mutations in the extracellular matrix protein collagen VI give rise to three serious skeletal muscle disorders: Bethlem myopathy, Ullrich congenital muscular dystrophy, and congenital myosclerosis [26]. Mitochondrial Ca^{2+} overload is regarded to play a key role in the pathogenesis of these muscular dystrophies. Muscle defects in collagen VI-deficient mice as well as in patients with collagen VI mutation-dependent muscular dystrophies are mitigated by pharmacological inhibition of the mitochondrial matrix protein peptidyl-prolyl cis-trans isomerase F (PPIF, NP_598845; also called cyclophilin D), a treatment that is considered to inhibit the Ca^{2+}-dependent opening of the mitochondrial permeability transition pore [27-30].

In mammals, each muscle fibre is under the direct control of a single branch of an α-motoneuron and hence its cellular activation occurs independently of the activity of neighbouring muscle fibres. Thus, studies on isolated single muscle fibres will reflect the function of muscle fibres *in vivo* and are therefore highly valuable in mechanistic studies of, for instance, the intracellular signalling associated with muscle activation and contraction. Single mouse flexor digitorum brevis (FDB) fibres can be isolated by collagenase treatment, a method that is relatively easy to use and hundreds of functional cells can be obtained from a single muscle[22, 31-35]. Alternatively, single FDB fibres can be obtained by mechanical microdissection, which is technically more intricate and only few functional fibres can be obtained from each muscle[36]. The immediate ECM and tendons are kept intact with mechanical microdissection, whereas enzymatic dissociation inevitably disturbs extracellular structures. Here, we used this difference between enzymatic dissociation and mechanical dissection to study the hypothesis that acute ECM disruption will affect muscle fibre structure and its ability to control mitochondrial Ca^{2+} influx during contraction-associated increases in $[Ca^{2+}]_{cyt}$.

Results

Intact links between ECM and cytoskeleton are necessary for the maintenance of skeletal muscle fibre structure

To examine the effects of the extracellular microenvironment on cellular phenotype, we compared mechanically dissected mouse flexor digitorum brevis (FDB) fibres with fibres isolated by conventional enzymatic dissociation using collagenase. Mechanical microdissection permits the isolation of fully viable muscle fibres with intact tendons and sarcolemma [36], including the adjacent ECM scaffold with preserved focal adhesion complexes, whereas physiological ECM contacts would be dissolved in enzymatically-isolated fibres. We first examined whether the different isolation methods translated into differences in cell morphology. In an initial set of experiments, we applied multi-photon-based Second Harmonic Generation (SHG) imaging and a quantitative morphometry technique to assess possible alterations in the myofibrillar architecture induced by the collagenase treatment [37]. SHG microscopy on single mechanically dissected FDB fibres revealed a complex outline of myofibrillar architecture with well-defined longitudinal ridges and valleys. Enzymatically dissociated fibres, on the other hand, were more homogeneously delineated with cross-sections approximating a circular shape and with shorter and more evenly extended sarcomeres (1.95 ± 0.005 µm; 72 measurements in 13 fibres) than in mechanically dissected fibres (2.08 ± 0.05 µm; 32 measurements in 5 fibres; $P = 0.015$) (Figure 1A; Video 1 & 2).

To further quantify the structural difference between mechanically dissected and enzymatically dissociated fibres, we quantified the cosine angle sum (CAS) in SHG images as a measure of a fibre's myofibrillar alignment, where CAS = 1 represents a perfectly linear parallel pattern, while CAS = 0 reflects perpendicularly oriented structures [37, 38]. Notably, the cosine angle sum was significantly higher for enzymatically dissociated fibres than for mechanically dissected, corroborating the observation of homogeneously striated patterns and parallel myofibrillar alignment in dissociated fibres with little interruption by longitudinal ridges and valleys, which were typical features in dissected fibres (Figure 1B).

It is well established that the structural linkage between the ECM and the cytoskeleton has a crucial role in cell signalling [18], and defects in this linkage underlie the disease progression in several muscular dystrophies [24, 25]. Therefore, we assessed whether the disruption of ECM contacts by enzymatic digestion affected the expression of key genes encoding for structural proteins. Interestingly, gene expression levels for collagen VI, desmin, dystrophin, laminin 2 and titin were all significantly lower in enzymatically dissociated than in mechanically dissected fibres (Figure 1C).

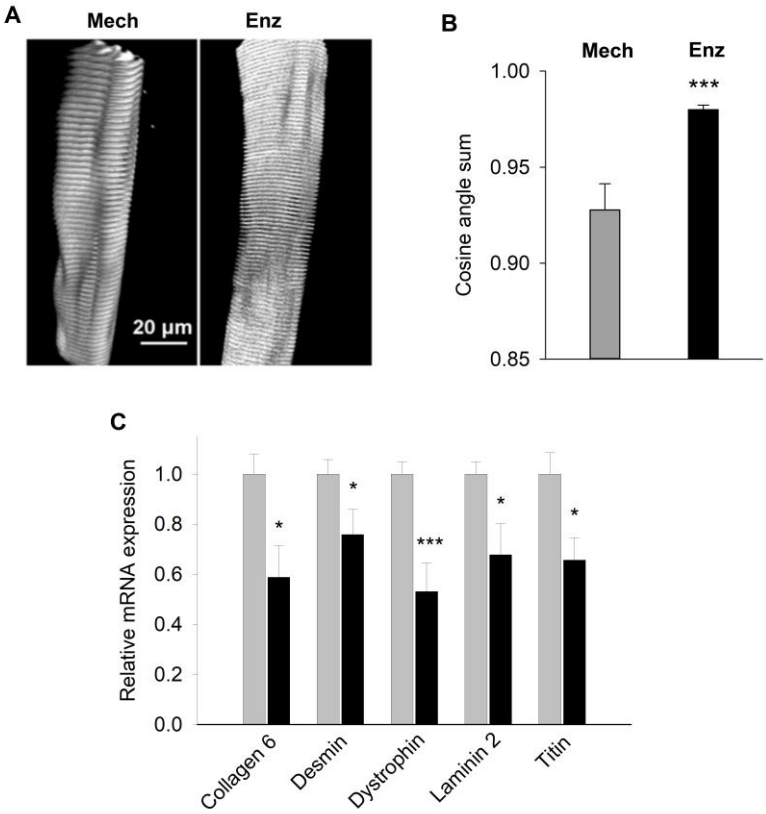

Figure 1**. **Disruption of the extracellular matrix results in altered cell shape and downregulation of genes encoding for structural proteins.
*(**A**) Representative SHG images from a mechanically dissected (Mech) and an enzymatically dissociated (Enz; using collagenase) mouse FDB fibre. Scale bar, 20 µm. (**B**) Average data of the cosine angle sum of mechanically dissected (n = 5) and enzymatically dissociated (n = 13) fibres. (**C**) Relative mRNA expression of genes encoding for structural proteins in mechanically dissected fibre bundles (n = 11) and enzymatically dissociated fibres (n = 6); mean expression in dissected fibres set to 1.0. Grey bars = mechanically dissected fibres; black bars = enzymatically dissociated fibres; all experiments were performed 4 hours after muscle fiber isolation. * P < 0.05 and *** P < 0.001 vs. mechanically dissected fibres with unpaired t-test. Data are presented as mean ± SEM.*

Possible collagenase-induced alterations in mitochondrial shape and spatial organization were addressed by electron microscopy on muscle fibres fixed 4 hours after being mechanically dissected or enzymatically dissociated. In an initial set of experiments, ultrathin sections were imaged and analysed with respect to mitochondrial cross-sectional area using transmission electron microscopy (TEM; Figure 2A-B). This analysis revealed no apparent difference between the two groups with average mitochondrial cross-sectional areas being 0.042 μm^2 in mechanically dissected and 0.052 μm^2 in enzymatically dissociated fibres (Figure 2C). However, traditional TEM on thin section does

not provide information on mitochondrial 3D structure and volume. We therefore used image volumes acquired by focused ion beam scanning electron microscopy (FIB-SEM) to look at mitochondrial distribution in a tissue volume [39, 40]. By sequential FIB milling of 30 nm slices, 3D mitochondrial models in fibre volumes of 365 μm^3 (7.9 x 4.5 x 10.3 µm) were obtained from a mechanically dissected and an enzymatically dissociated fibre (Figure 2D-G; Video 3 & 4). The 3D images look grossly similar in the two fibres, but a detailed analysis revealed longer and more branched mitochondria in the mechanically dissected than in the enzymatically dissociated fibre. Accordingly, the total mitochondrial volumes in the two models were similar (20.2 *vs*. 17.1 μm^3, corresponding to 5.5% *vs*. 4.6% of the total fibre volume), whereas the number of mitochondria was clearly lower (86 *vs*. 140) and their average volume larger in the mechanically dissected (0.235 μm^3) than in the enzymatically dissociated (0.122 μm^3) fibre.

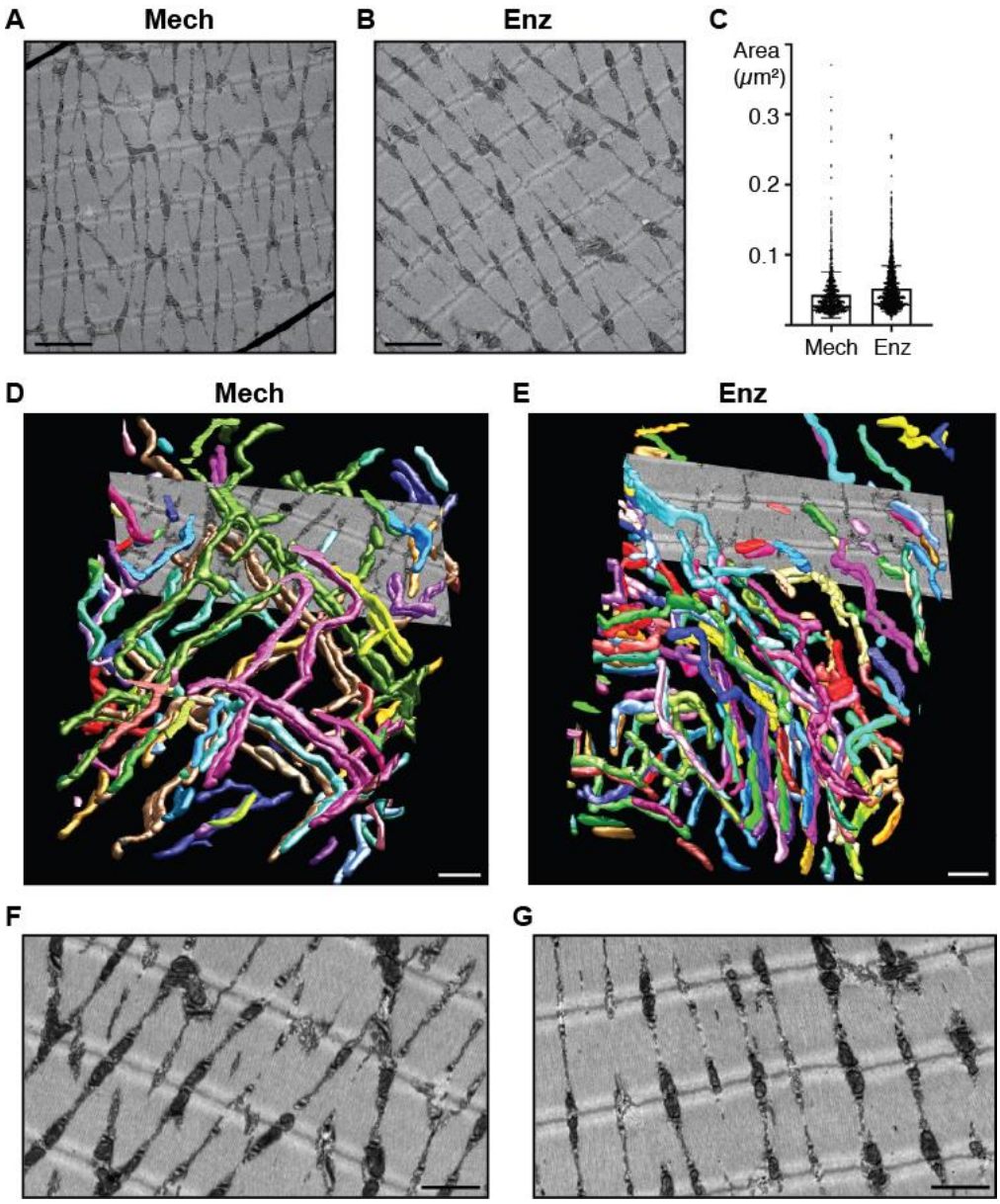

***Figure 2*. Disruption of the extracellular matrix causes subtle changes in mitochondrial morphology as detected with 3D electron microscopy.**

*Representative TEM images of a mechanically dissected (**A**) and a collagenase dissociated (B) FDB muscle fibre. Scale bar in A and B is 2 µm. (**C**) Graphical presentation of individual and mean (± SD) mitochondrial areas measured from TEM images acquired from mechanically dissected fibres (left; n=1154 mitochondria in 20 images of distinct areas of 6 fibres) and enzymatically dissociated fibres (right, n=1390 mitochondria in 20 images of distinct areas of 10 fibres). 3D model of the mitochondria in a volume of 365 µm^3 muscle tissue obtained with FIB-SEM in a dissected fibre (**D**) and collagenase-treated fibre (**E**); rotating 3D models are presented in Videos 3 & 4. Individual mitochondria are distinguished by different colours; scale bar D and E is 1 µm. Representative images from slices used in the FIB-SEM-based modelling acquired in the dissected (**F**) and the collagenase-treated (**G**) fibre, respectively. Fibres were fixed 4 hours after being isolated. Scale bar F and G is 1 µm.*

Collagenase treatment results in aberrant mitochondrial Ca^{2+} uptake

Next, we investigated whether collagenase-induced disturbance of the ECM would impact cellular Ca^{2+} handling. We previously showed that repeated tetani do not result in markedly increased $[Ca^{2+}]_{mit}$ in mechanically dissected FDB muscle fibres of wild-type mice [41]. Intriguingly and in sharp contrast to mechanically dissected fibres, we noticed a marked increase in $[Ca^{2+}]_{mit}$, as indicated by an increased fluorescence signal of the mitochondrial Ca^{2+} indicator rhod-2, when FDB fibres were isolated by conventional enzymatic digestion (Figure 3A). Importantly, these differences in mitochondrial Ca^{2+} control between mechanically dissected and enzymatically dissociated FDB fibres were not due to differences in tetanic $[Ca^{2+}]_{cyt}$ (Figure 3B). Four hours after enzymatic dissociation, FDB fibres showed more than doubling of the rhod-2 fluorescence immediately after 25 brief (350 ms duration, given at 2 s interval) tetani, and a similar increase was observed in fibres studied 24 and 48 hours after enzymatic dissociation (Figure 3C). By contrast, four hours after mechanical dissection, $[Ca^{2+}]_{mit}$ was only marginally increased after repeated tetanic stimulation in fibres that were either contracting isometrically or that were shortening freely, i.e. exposed to contraction conditions identical to those of enzymatically dissociated fibres. However, another picture emerged after collagenase treatment of mechanically dissected fibres, where the repeated contractions resulted in an increase of $[Ca^{2+}]_{mit}$ that reached levels comparable to those observed in the enzymatically dissociated fibres.

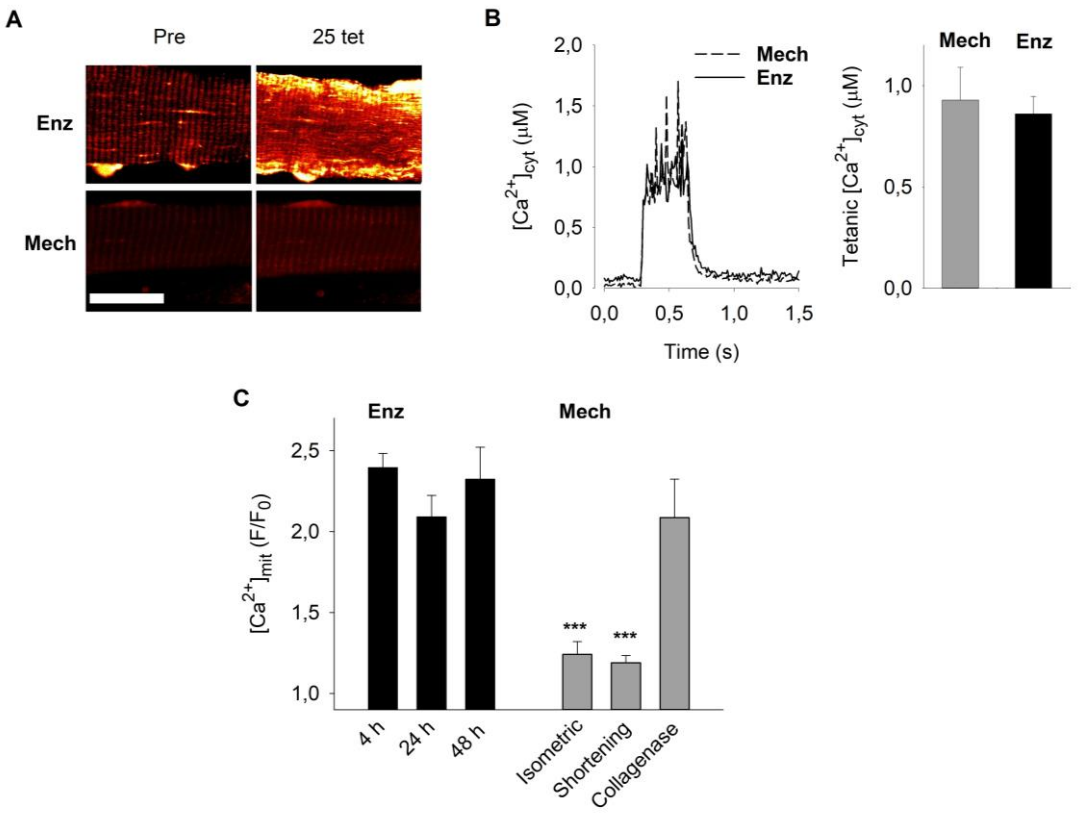

Figure 3. Loss of mitochondrial Ca^{2+} control in enzymatically dissociated muscle fibres.

*(**A**) Representative rhod-2 fluorescence images of enzymatically dissociated (Enz) and mechanically dissected (Mech) mouse FDB fibres before and after 25 brief tetanic contractions. Scale bar, 20 µm. (**B**) Average $[Ca^{2+}]_{cyt}$ records (left) and mean tetanic $[Ca^{2+}]_{cyt}$ (right) during tetanic stimulation (70 Hz, 350 ms duration) of enzymatically dissociated (solid line and black bar) and mechanically dissected (dashed line and grey bar) FDB fibres (n = 6 in both groups). (**C**) Mean data of rhod-2 fluorescence immediately after (F) relative to before (F_0) 25 repeated tetani in enzymatically dissociated fibres stored for 4-48 hours after isolation (black bars) and in fibres studied 4 hours after mechanical dissection either contracting isometrically, shortening freely, or after collagenase treatment (grey bars). *** $P < 0.001$ vs. 4 hours dissociated fibres with one-way ANOVA ($n \geq 5$). Data are presented as mean ± SEM.*

Mitochondrial Ca^{2+} uptake in enzymatically dissociated fibres is mediated via MCU- and PPIF-dependent pathways

Next, we assessed the molecular mechanisms by which Ca^{2+} entered mitochondria in enzymatically dissociated cells. The ruthenium red subcomponent Ru360 constitutes an effective inhibitor of MCU-mediated mitochondrial Ca^{2+} entry [42]. While Ru360 specifically inhibits MCU in experiments on isolated mitochondria, its limited plasma membrane permeability limits its use in intact cell systems

[43]. Therefore, enzymatically dissociated FDB fibres were first microinjected with Ru360 and subsequently superfused by Ru360 for 30 minutes before commencing the repeated tetanic stimulation. Notably, Ru360 treatment significantly decreased but did not abrogate the tetanic stimulation-induced increase in $[Ca^{2+}]_{mit}$ (Figure 4A,B).

Cyclosporin A (CsA) is a cyclic endecapeptide calcineurin inhibitor that is widely used in clinical practice as an oral immunosuppressant to prevent rejection of organ transplants and mitigate symptoms in various autoimmune diseases [44]. CsA binds to the mitochondrial protein PPIF (cyclophilin D) [45, 46] and counteracts the opening of the mitochondrial permeability transition pore [47-50]. In addition, CsA has been shown to reduce mitochondrial Ca^{2+} uptake in mitochondrial myopathy muscle fibres exposed to repeated tetanic stimulation and in ischemic rabbit cardiomyocytes [41, 51, 52]. The increase in $[Ca^{2+}]_{mit}$ was markedly blunted when enzymatically dissociated FDB fibres were exposed to 25 repeated tetani in the presence of CsA (Fig. 4A,B). In fact, the reduction of mitochondrial Ca^{2+} uptake observed with CsA was similar to that with Ru360. Measurements of $[Ca^{2+}]_{cyt}$ showed no effect of CsA either at rest or during tetanic stimulation (Fig. 4C-E).

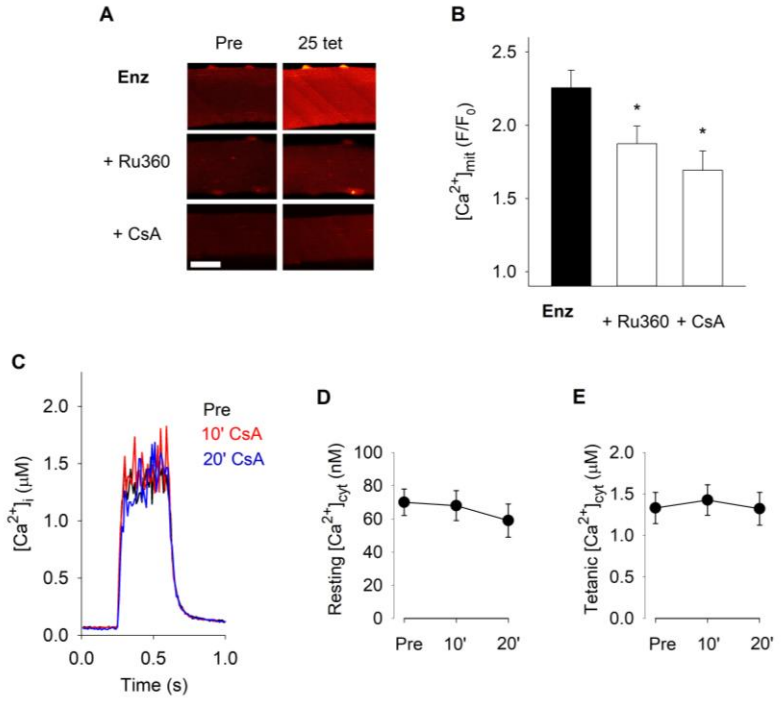

Figure 4. Aberrant mitochondrial Ca^{2+} uptake in enzymatically dissociated muscle fibres is mitigated by pharmacological inhibition of MCU and PPIF.

*(**A**) Representative rhod-2 fluorescence images of enzymatically dissociated FDB fibres obtained before (Pre) and after 25 brief tetanic contractions produced either under control conditions or in the presence of Ru360 (microinjected plus 10 µM superfusion) or cyclosporin A (CsA; 1.6 µM). Scale bar, 20 µm. (**B**) Mean data of the increase in rhod-2 fluorescence after (F) relative to before (F_0) 25 repeated tetani; * $P < 0.05$ vs. control (Enz) with one-way ANOVA ($n \geq 13$). (**C**) Superimposed average $[Ca^{2+}]_{cyt}$ records obtained in eight FDB fibres during tetanic stimulation (70 Hz, 350 ms duration) before (Pre) and after 10 and 20 min exposure to CsA (1.6 µM). Mean data of $[Ca^{2+}]_{cyt}$ at rest (**D**) and during the tetanic stimulation (**E**); one-way repeated measures ANOVA shows no effect of CsA exposure on either resting ($P = 0.3$) or tetanic ($P = 0.5$) $[Ca^{2+}]_{cyt}$ ($n = 8$). Experiments were performed 4 hours after fibre isolation. Data are presented as mean ± SEM.*

To further assess the involvement of PPIF-related mitochondrial Ca^{2+} uptake, we complemented the analysis using the novel, more specific cyclophilin inhibitor, NV556 [53]. Importantly, $[Ca^{2+}]_{mit}$ was markedly lower during repeated tetani as well as in the subsequent recovery period in the presence than in the absence of NV556 (Figure 5A,B). In accordance with the results obtained with CsA, application of NV556 exposure had no effect on $[Ca^{2+}]_{cyt}$ at rest or during tetanic stimulation (Fig. 5C-E). Thus, pharmacological PPIF inhibition did not affect $[Ca^{2+}]_{cyt}$ and hence the driving force for mitochondrial Ca^{2+} entry. To sum up, these results support a model in which the isolation of muscle

fibres from their native external microenvironment causes increases in cytosolic Ca^{2+} to spill over into the mitochondrial matrix and this aberrant mitochondrial Ca^{2+} uptake involves the MCU and PPIF.

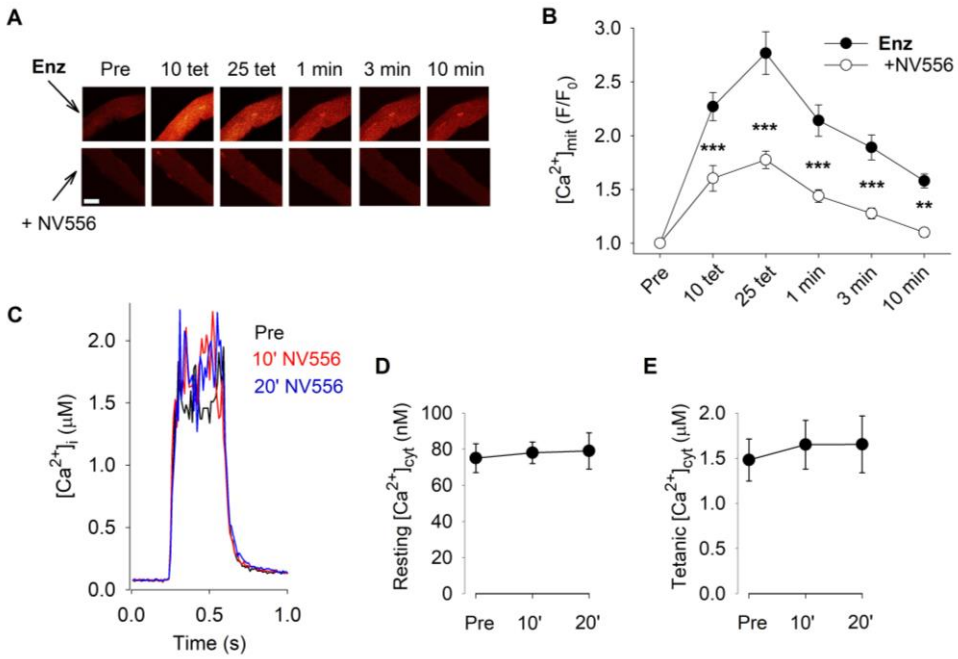

Figure 5. Aberrant mitochondrial Ca^{2+} uptake in enzymatically dissociated muscle fibres is mitigated by the cyclophilin inhibitor NV556.

*Representative rhod-2 fluorescence images (**A**) and quantification of the relative increase in fluorescence (**B**) of enzymatically dissociated FDB fibres stimulated with 25 repeated tetani either under control conditions or in the presence of the cyclophilin inhibitor NV556 (5 µM); ** P < 0.01, *** P < 0.001 vs. control with two-way repeated measures ANOVA (n ≥ 24). Scale bar, 20 µm. (**C**) Superimposed average $[Ca^{2+}]_{cyt}$ records obtained in nine FDB fibres during tetanic stimulation (70 Hz, 350 ms duration) before (Pre) and after 10 and 20 min exposure to NV556 (5 µM). Mean data of $[Ca^{2+}]_{cyt}$ at rest (**D**) and during the tetanic stimulation (**E**); one-way repeated measures ANOVA shows no effect of CsA exposure on either resting (P = 0.7) or tetanic (P = 0.5) $[Ca^{2+}]_{cyt}$ (n = 9). Experiments were performed 4 hours after fibre isolation. Data are presented as mean ± SEM.*

The aberrant mitochondrial Ca^{2+} uptake upon enzymatic dissociation does not cause acute mitochondrial dysfunction

Notably and consistent with previous reports [31], repeated contractions did not affect the mitochondrial membrane potential ($\Delta\psi_m$) in enzymatically dissociated muscle fibres, as assessed by the fluorescent indicator tetra-methyl rhodamineethylester (TMRE) (Figure 6A,B). In contrast, application of the mitochondrial uncoupler carbonyl cyanide-4-(trifluoromethoxy) phenylhydrazone

(FCCP) showed a marked depolarization of $\Delta\psi_m$ as indicated by decreased TMRE fluorescence to ~30% of the baseline value. Furthermore, extensive mitochondrial Ca^{2+} uptake results in accelerated production of reactive oxygen species (ROS), which can have deleterious effects on cell function [8]. We used the fluorescent indicator MitoSOX Red to measure an increase in preferentially mitochondrial production of superoxide (O_2^{*-}) [41]. Mean MitoSOX Red fluorescence was marginally increased by 18 ± 1% (n = 8; *P* = 0.08; paired t-test) in enzymatically dissociated fibres after 25 repeated tetanic contractions, whereas exposure to 1 mM H_2O_2 resulted in a several-fold increase in MitoSOX Red fluorescence (Figure 6C). These findings imply that the observed increases in $[Ca^{2+}]_{mit}$ upon enzymatic dissociation remained within the physiological range and did not reach levels high enough to trigger acute mitochondrial depolarization or acute oxidative stress.

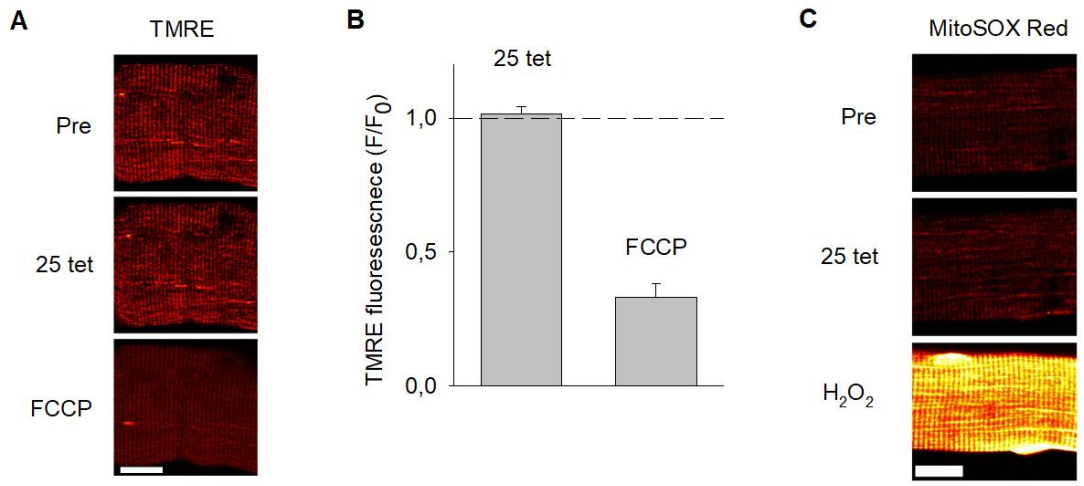

Figure 6. Enzymatic dissociation does not cause mitochondrial depolarization or increased ROS production.

*(A) Representative TMRE fluorescence images and (**B**) mean data (± SEM) show no significant increase in TMRE fluorescence after (F) relative to before (F_0) 25 repeated tetani, whereas the subsequent exposure to the mitochondrial uncoupler FCCP (1 µM) resulted in a marked decrease in fluorescence (n = 17). (**C**) Representative images show no clear increase in MitoSOX Red fluorescence after 25 contractions, whereas fluorescence increased several-fold during the subsequent exposure to 1 mM H_2O_2. Experiments were performed 4 hours after fibre isolation. Scale bars in **A** and **C**, 20 µm.*

Enzymatic dissociation masks mitochondrial Ca^{2+} handling defects in mitochondrial myopathy muscle fibres.

Fast-twitch skeletal muscle fibre-specific mitochondrial transcription factor A knock-out (*Tfam* KO) mice display important hallmarks of severe mitochondrial myopathy [54]. In agreement with previous results [41, 51], repeated tetanic stimulation resulted in a marked increase in $[Ca^{2+}]_{mit}$ in mechanically dissected *Tfam* KO FDB fibres but not in fibres dissected from their littermate controls (Figure 7A). Note that the increased mitochondrial Ca^{2+} uptake in *Tfam* KO fibres occurred despite a reduced driving force for Ca^{2+} into the mitochondrial matrix due to lower tetanic $[Ca^{2+}]_{cyt}$ in *Tfam* KO than in control fibres (Figure 7B) [41, 51]. Importantly, when enzymatic dissociated fibres were exposed to the repeated tetanic stimulation, fibres of both groups showed a marked increase in $[Ca^{2+}]_{mit}$ and hence the difference in mitochondrial Ca^{2+} uptake between *Tfam* KO and control fibres was lost.

Treatment with CsA has been shown to counteract the development of muscle weakness and prolong the lifespan of the *Tfam* KO mice [51]. We here tested whether PPIF inhibition using the specific cyclophilin inhibitor NV556 also improves survival of the *Tfam* KO mice. NV556 was delivered via osmotic pumps and treatment started at an age of 14 weeks when the *Tfam* KO mice are about to enter the terminal state with severe weight loss and muscle weakness [51]. The osmotic pumps were estimated to deliver ~140 µg NV556 per day for up to 6 weeks. At the end of the treatment period, 17 out of 18 treated mice were still alive, whereas only 7 out of 14 untreated mice were alive (P = 0.015; z-test; Figure 7C). Notably, the beneficial effects on survival were rapidly lost after the end of treatment and all mice were dead 9 weeks after the implantation of osmotic pumps, i.e. after 3 weeks without treatment (data not shown). These data imply that pharmacological inhibition of excessive mitochondrial Ca^{2+} uptake improves outcomes in a mouse model of lethal mitochondrial myopathy.

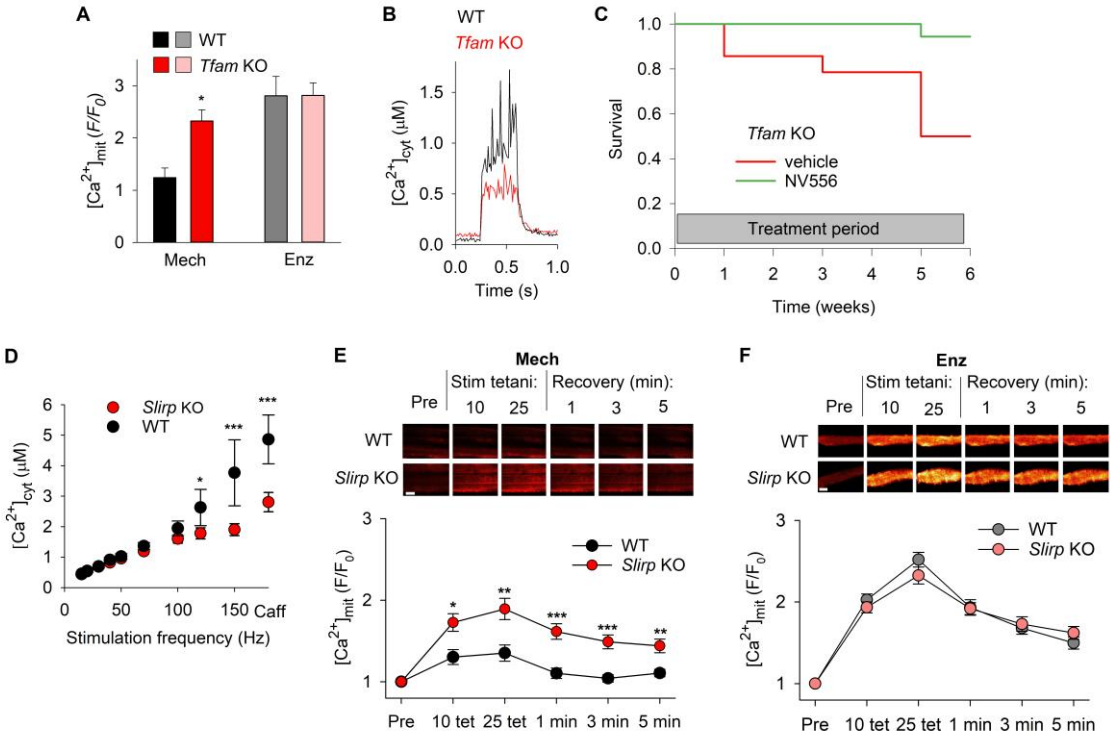

Figure 7. The aberrant contraction-induced mitochondrial Ca^{2+} uptake in mitochondrial myopathy muscle fibres eludes detection in enzymatically dissociated fibres.

*(**A**) Mean data of the relative increase in rhod-2 fluorescence after 25 repeated tetanic contractions in mechanically dissected (Mech) Tfam KO (n = 5) and littermate controls (WT; n = 3) or enzymatically dissociated (Enz) Tfam KO (n = 10) and WT (n = 4) FDB fibres. * P < 0.05 vs. WT with unpaired t-test. (**B**) Superimposed average $[Ca^{2+}]_{cyt}$ records during tetanic stimulation (70 Hz, 350 ms duration) obtained in mechanically dissected FDB fibres of control mice (WT, n = 6 fibres; same data as in Fig. 3B) and Tfam KO mice (n = 4 fibres). (**C**) Survival curves Tfam KO mice treated with the PPIF inhibitor NV556 that blocks mitochondrial Ca^{2+} uptake (140 µg daily; green line) or with vehicle control (red line) using osmotic pumps for up to 6 weeks (treatments started at an age of 14 weeks). (**D**) Mean data of cytosolic free $[Ca^{2+}]$ ($[Ca^{2+}]_{cyt}$) during brief stimulations at different frequencies and in the presence of caffeine (Caff, 5 mM) of WT (n = 7) and Slirp KO (n = 11) FDB fibres. Representative rhod-2 fluorescence images of a small bundle of mechanically dissected (**E**) and enzymatically dissociated (**F**) FDB fibres of WT and Slirp KO mice obtained before (Pre) and after 10 and 25 repeated tetanic stimulation and at 1, 3 and 5 minutes of recovery (scale bars, 20 µm). Lower parts of E and F show mean data of the stimulation-induced relative increase in rhod-2 fluorescence (n ≥ 19). Experiments were performed 4 hours after fibre isolation. * P < 0.05, ** P < 0.01, *** P < 0.001 vs. WT with two-way repeated measures ANOVA. Data are presented as mean ± SEM.*

Intrigued by fact that the aberrant mitochondrial Ca^{2+} uptake in *Tfam* KO fibres eluded detection in enzymatically dissociated fibres, we performed experiments on another mouse model with defective mitochondria, that is, mice deficient of stem-loop interacting RNA binding protein (SLIRP) [55]. Despite a 50–70% reduction in the steady-state levels of mtDNA-encoded mRNAs, *Slirp* KO mice appear largely healthy with only minor (~5%) reduction in body weight [55]. The $[Ca^{2+}]_{cyt}$-frequency relationship was studied in FDB fibres mechanically dissected from *Slirp* KO mice and wildtype littermates by producing brief contractions at 1 minute intervals. *Slirp* KO fibres displayed lower $[Ca^{2+}]_{cyt}$ than wildtype fibres at high stimulation frequencies (120-150 Hz) and during tetanic stimulation in the presence of caffeine (5 mM), which facilitates SR Ca^{2+} release and hence provides an estimate of the total amount of Ca^{2+} stored in the SR (Figure 7D) [56]. These results indicate a reduced SR Ca^{2+} storage capacity in *Slirp* KO muscle, which agrees with previous results obtained in *Tfam* KO fibres [41, 51]. Thus, a decreased SR Ca^{2+} storage capacity is a common feature in muscle fibres of mice with two completely different genetically engineered mitochondrial defects.

In accordance with the results from *Tfam* KO muscle fibres, rhod-2 fluorescence increased more during 25 repeated tetanic contractions in mechanically dissected *Slirp* KO than in wildtype muscle fibres (Figure 7E). Importantly, these differences between *Slirp* KO and wildtype fibres were masked by substantial increases in $[Ca^{2+}]_{mit}$ in the wildtype group when experiments were performed with enzymatically dissociated fibres (Figure 7F). Thus, two mitochondrial myopathy mouse models, *Slirp* KO and *Tfam* KO, both showed augmented mitochondrial Ca^{2+} uptake during repeated contractions despite decreased SR Ca^{2+} storage and hence, if anything, decreased $[Ca^{2+}]_{cyt}$ during tetanic contractions. Importantly, isolation of wildtype muscle fibres by enzymatic ECM digestion resulted in perturbed mitochondrial Ca^{2+} handling that resembled the defective Ca^{2+} handling observed in mitochondrial myopathy models. As a consequence, differences in mitochondrial Ca^{2+} uptake between enzymatically digested wildtype and myopathy fibres could no longer be detected. However, isolating muscle fibres by microdissection, which preserves their extracellular microenvironment, allowed detection of the aberrant mitochondrial Ca^{2+} uptake in *Tfam* KO as well as in *Slirp* KO muscle fibres.

Discussion

In vitro cell studies constitute essential tools for studies of cell biology, morphogenesis, phenotype characterization, and drug development. However, an increasing body of evidence highlights the fact that isolating cells by enzymatic dissociation and subsequently study them under conventional 2D monolayer conditions entails the rapid loss of adult cellular phenotypes, which confounds result interpretation and impairs the translation of findings [57]. Enzymatic dissociation of cells disturbs

integrin-mediated cell adhesions, which provide dynamic connections between the ECM and the intracellular cytoskeleton that are involved in the control of cell structure, including the morphology and function of mitochondria [18-20]. In this study, we provide a link between enzymatic disruption of the ECM, altered cell structure and defective control of mitochondrial Ca^{2+} uptake. Specifically, enzymatically dissociated muscle fibres failed to limit mitochondrial Ca^{2+} influx during a series of increases in $[Ca^{2+}]_{cyt}$ induced by repeated tetanic stimulation. Conversely, the control of $[Ca^{2+}]_{mit}$ was maintained when muscle fibres were isolated by mechanical dissection, which leaves the immediate ECM intact.

SHG imaging revealed a less elaborate cell structure in enzymatically dissociated than in mechanically dissected fibres. Moreover, the expression of genes encoding for structural proteins was markedly lower in enzymatically dissociated than in mechanically dissected fibres. Conventional thin section EM did not expose any striking ultrastructural difference in mitochondrial shape and cross-sectional area between the two groups of fibres. However, FIB-SEM showed subtle differences in the mitochondrial 3D network with the total mitochondrial volume being similar in the two groups, whereas the number of mitochondria being higher and consequently the volume of individual mitochondria lower in enzymatically dissociated fibres, hence supporting an important role of the ECM in the control of the dynamic balance between mitochondrial fusion and fission [58-60]. To sum up, collagen-mediated ECM disruption had clear-cut acute effects on cellular structure and the maintenance of structural proteins, whereas the effects on mitochondrial network structure were more subtle. Accordingly, the aberrant mitochondrial Ca^{2+} uptake during repeated tetanic contractions of enzymatically dissociated fibres was within the short-term “physiological” range and not accompanied by any acute mitochondrial depolarization or increased ROS production, both regarded as important consequences of severe mitochondrial distress [8-10].

Our results imply a PPIF-dependent mitochondrial Ca^{2+} uptake in enzymatically dissociated muscle fibres because the excessive increase in $[Ca^{2+}]_{mit}$ in response to increased $[Ca^{2+}]_{cyt}$ was significantly decreased by CsA and NV556. Interestingly, previous studies show that myopathies in mice deficient in the ECM protein collagen VI could be counteracted by CsA [29] and the non-immunosuppressive PPIF inhibitor alisporivir (also called Debio 025) [30]. Thus, our data suggest that the adverse effects of a disturbed ECM microenvironment on cellular phenotypes are mediated via impaired PPIF-dependent fine-tuning of intracellular Ca^{2+} signalling. Critically, we here show that pharmacological inhibition of the aberrant mitochondrial Ca^{2+} uptake with NV556 improved survival in *Tfam* KO mice, a mouse model of lethal mitochondrial myopathy, which corroborates with the previously reported prolonged survival when these mice were treated with CsA [51].

The presented findings highlight multiple important implications for the study of cell biological phenomena *in vitro*. Firstly, our data emphasize the importance of using cell culture systems that preserve the immediate ECM to ensure that results faithfully reflect *in vivo* processes. Secondly, enzymatic digestion rapidly changes the molecular phenotypes and functionality of cells. For instance, recent studies have shown redundant activation of muscle stem cells isolated from adult skeletal muscle with standard enzymatic dissociation protocols, which has important consequences for the use of these cells as quiescent controls [61, 62]. Thirdly, dissolving the microphysiological niche around cells can result in perturbations that resemble pathological phenotypes observed in mitochondrial disease. Specifically, the pathognomonic increase in $[Ca^{2+}]_{mit}$ during repeated contractions of muscle fibres in mitochondrial myopathy would be missed in experiments performed on enzymatically dissociated cells. Thus, enzymatically dissociated cells should be avoided as experimental paradigm for the study of diseases that potentially involve altered mitochondrial Ca^{2+} signalling.

In conclusion, disruption of the immediate ECM by collagenase treatment results in loss of the fine-detailed cell structure of muscle fibres and impaired control of mitochondrial Ca^{2+} uptake, which involves a PPIF-dependent mitochondrial Ca^{2+} influx resembling that observed in mitochondrial myopathies. Our results support a central role of mitochondrial Ca^{2+} as a critical mediator that links the native extracellular microenvironment to the maintenance of normal cellular structure and function.

Materials and methods

Animals. C57bl/6J female mice were used, except when stated otherwise. Fast-twitch skeletal muscle fibre-specific *Tfam* KO mice and their controls were generated as described previously [54]. *Slirp* KO mice and wildtype littermates were generated as described previously [55]. Mice were euthanized by rapid neck disarticulation and the FDB muscles were excised. All animal experiments were approved by the Stockholm North Local Animal Ethics Committee.

Some *Tfam* KO mice were treated with the specific cyclophilin inhibitor, NV556 [53], or vehicle only. NV556 was dissolved to 40 mg/ml in cyclodextrin formulation (pH 7.4). Mini-osmotic pumps (Alzet model 2006) were loaded with approximately 200 µl of either dissolved NV556 or cyclodextrin formulation only and incubated in sterile PBS for 48 hours prior to implantation. The mini-osmotic pumps were implanted subcutaneously on the back of mice under isoflurane anaesthesia. Mice were weighed 48 hours after surgery; body weight was then monitored twice per week for the remainder of the experiment period. Mice were regarded as terminally ill and euthanized either at loss of 20% bodyweight or severe loss of muscle functionality. Mice were euthanized by rapid neck dislocation.

Enzymatic dissociation and mechanical dissection of FDB fibres. Flexor digitorum brevis (FDB) muscles were cleaned of tendons, connective tissue, and blood vessels and incubated for ~2 hours at 37°C in 0.3% collagenase type I (Sigma) in Dulbecco´s modified Eagle medium (DMEM; Invitrogen) supplemented with 20% fetal bovine serum. Muscles were then transferred to fresh DMEM and gently triturated to dissociate individual muscle fibres. A volume of 300 µl of the resultant muscle fibre suspension was placed in laminin-coated glass-bottom Petri dishes, and fibres were allowed to attach for up to 15 minutes. Thereafter, 3 ml DMEM supplemented with antibiotic, antimycotic solution (1 µL/ml, Sigma) was added. Experiments were performed ~4 hours after enzymatic dissociation, except when otherwise noted.

Single or small bundles (2-5 fibres) of FDB fibres were mechanically dissected as previously described [36]. In one set of experiments (see Figure 2C), dissected fibres were subjected to the same enzymatic dissociation protocol as the dissociated fibres with the exception that no trituration was performed.

Confocal measurements with fluorescent indicators in FDB fibres. For mitochondrial [Ca^{2+}] ($[Ca^{2+}]_{mit}$), membrane potential ($\Delta\psi_m$) and ROS production measurements (see below), loading of

fluorescent indicators followed by wash-out was performed at room temperature for 20 minutes. During FDB fibre experiments, cells were superfused at room temperature (~25°C) with Tyrode solution (in mM): NaCl, 121; KCl, 5.0; $CaCl_2$, 1.8; $MgCl_2$, 0.5; NaH_2PO_4, 0.4; $NaHCO_3$, 24.0; EDTA, 0.1; glucose, 5.5; 0.2% fetal calf serum. The solution was bubbled with 95% O_2–5% CO_2. Measurements were performed using a BioRad MRC 1024 confocal unit with a dual Calypso laser (Cobolt, Solna, Sweden) attached to a Nikon Diaphot 200 inverted microscope. Confocal images were obtained before and after 10 and 25 repeated tetani (70 Hz, 350 ms stimulation trains given at 2 s intervals) and at regular intervals after the contractions. Confocal images were analysed using ImageJ and data are expressed as F/F_0, i.e. the ratio of the fluorescence intensity after and before the repeated contractions, respectively.

$[Ca^{2+}]_{mit}$. Fibres were incubated in 5 µM rhod-2 in the membrane permeable AM form (Invitrogen). Rhod-2 was excited with 531 nm light and the emitted light was collected through a 585 nm long-pass filter.

$\Delta\psi_m$. Fibres were incubated in 1 µM TMRE (Invitrogen). TMRE was excited at 531 nm and the emitted light was collected through a 605 nm long-pass filter. Approximately 30 minutes after completion of the 25 repeated tetani, fibres were exposed to 1 µM FCCP (Sigma) to significantly depolarize the mitochondria and confocal images were obtained.

Mitochondrial ROS production. Fibres were loaded with 5 µM MitoSOX Red (Invitrogen). MitoSOX Red was excited with 488 nm light and emitted light was collected through a 585 nm long-pass filter. As a positive control, 1 mM H_2O_2 was applied at the end of experiments to increase mitochondrial superoxide by inducing product inhibition of superoxide dismutase 2 [63, 64], and confocal images were obtained every minute until the MitoSOX Red signal reached a plateau.

Ru360, CsA and NV556 experiments. Enzymatically dissociated FDB fibres were loaded with rhod-2 to measure $[Ca^{2+}]_{mit}$ as described above. To investigate the potential sites of Ca^{2+} entry into mitochondria, enzymatically dissociated fibres were exposed to either Ru360 (Calbiochem), CsA or NV556 (NeuroVive Pharmaceutical AB, Lund, Sweden). Ru360 was first injected into the fibres and they were subsequently superfused with 10 µM Ru360 throughout the experiment. CsA (1.6 µM; Novartis) or NV556 (5 µM) was applied to the fibres for 5 minutes before and during the 25 repeated tetani.

Single fibre $[Ca^{2+}]_{cyt}$ measurements. Intact single FDB fibres were mechanically dissected [36]. Aluminum clips were attached to the tendons and the fibre was mounted in a chamber between an Akers 801 force transducer (Kronex Technologies, Oakland, CA, USA) and an adjustable holder and subsequently superfused by Tyrode solution (see above) at room temperature. The fibre length was adjusted to obtain maximum tetanic force. The fibre was stimulated with supramaximal electrical pulses (0.5 ms in duration) delivered via platinum electrodes placed along the long axis of the fibre. The steady-state $[Ca^{2+}]_{cyt}$-frequency relationship was obtained by stimulating fibres for 350 ms at 15-150 Hz every 1 minutes; 150 Hz contractions were also produced in the presence of 5 mM caffeine to assess the SR Ca^{2+} storage capacity.

Fibres were microinjected with the fluorescent Ca^{2+} indicator indo-1 (Molecular Probes/Invitrogen, Carlsbad, CA, USA), or loaded with indo-1 AM in experiments on enzymatically dissociated fibres. The emitted fluorescence of indo-1 was measured with a system consisting of a Xenon lamp, a monochromator, and two photomultiplier tubes (Photon Technology International, Wedel, Germany). The excitation light was set to 360 nm, and the light emitted at 405 ± 5 and 495 ± 5 nm was measured by the photomultipliers. The ratio of the light emitted at 405 nm to that at 495 nm (R) was converted to $[Ca^{2+}]_{cyt}$ using the following equation:

$$[Ca^{2+}]_{cyt} = K_d\ \beta\ (R - R_{min})/(R_{max} - R),$$

where K_d is the apparent dissociation constant of indo 1, β is the ratio of the 495 nm signals at very low and saturating $[Ca^{2+}]_{cyt}$, R_{min} is the ratio at very low $[Ca^{2+}]_{cyt}$, and R_{max} is the ratio at saturating $[Ca^{2+}]_{cyt}$. Fluorescence was sampled online and stored on a computer for subsequent data analysis. $[Ca^{2+}]_{cyt}$ was measured at rest and as the mean during 70 Hz, 350 ms tetanic stimulation. The steady-state $[Ca^{2+}]_{cyt}$-frequency relationship was obtained in *Slirp* KO and control WT fibres by stimulating fibres for 350 ms at 15-150 Hz every 1 minutes; 150 Hz contractions were also produced in the presence of 5 mM caffeine to assess the SR Ca^{2+} storage capacity.

Second Harmonic Generation microscopy. FDB fibres were imaged using a multiphoton microscope (TriMScope II, LaVision BioTech, Bielefeld, Germany) equipped with a combination of two water immersion objectives (LD C-APO 40x/1.1 W Corr M27 on the excitation side, W Plan-APO 20x/1.0 DIC M27 on the transmission side, Zeiss) and a mode-locked ps-pulsed Ti:Sa-laser (Chameleon Vision II, Coherent, Santa Clara, CA) tuned to 810 nm to excite the myosin SHG signal [65, 66]. The SHG signal from myosin was separated from other (autofluorescence) signals by a band pass filter (405/20 nm, CHROMA, Bellows Falls, VT) and detected by a non-descanned photomultiplier (H7422-40, Hamamatsu Photonics, Hamamatsu, Japan). Muscle fibres were z-scanned (voxel-size: 0.14 x 0.14 x

0.3 µm) to detect the cosine angle sum based on boundary tensor analysis [37, 38]. Image processing was performed in MATLAB (MathWorks, Natick, MA).

Transmission Electron Microscopy.

Isolated FDB muscle fibres were fixed in 2.5% glutaraldehyde (TAAB Laboratories), 4% formaldehyde in 0.1 M sodium cacodylate buffer. All samples were processed using Pelco Biowave Pro+ microwave tissue processor (Ted Pella) according to [67], with minor modifications: no Ca^{2+} was used during the fixation and contrasting steps with lead aspartate was omitted to reduce overstaining. Samples were trimmed with a glass knife and 70 nm ultrathin sections were picked up on Cu-grids and examined with the TEM Talos L120C (FEI, currently Thermo Fischer Scientific) operating at 120 kV. Micrographs were acquired with a Ceta 16M CCD camera (FEI) using TEM Image & Analysis software ver. 4.17 (FEI).

For focused ion beam scanning electron microscopy (FIB-SEM), a small cube of the sample was cut and glued on a SEM stub with epoxy and silver glue. In the SEM chamber, the specimen was coated with a 5 nm thin layer of platinum to reduce charging. Specimen were imaged using Scios DualBeam SEM (FEI) and the 'Auto slice and view' software system; the electron beam operated at 2 kV and 0.2 nA and the T1 lens was used for detection. A 1 µm protective layer of platinum was deposited on the selected area before milling. FIB milling thickness was set to 30 nm and each slice was imaged with pixel sizes 3,55 x 3,55 nm (for mechanically dissected fibre) and 3,74 x 3,74 nm (for enzymatically dissociated fibre). Images were further processed using the ImageJ plugins 'Linear Stack Alignment with SIFT' and 'Multistackreg' and the mitochondrial network was reconstructed and analysed in a final volume of 365 μm^3 (7,9 x 4,5 x 10,3 µm). Identified mitochondrial volumes were modelled and measured using the IMOD software package ver. 4.9.13 [68].

Gene expression

Muscle RNA was isolated using TRIzol reagent (Life Technologies, Stockholm, Sweden). Gene expression analysis was performed by real-time quantitative PCR (qPCR) using iTaq Universal SYBR Green Supermix (Bio-Rad Laboratories AB, Solna, Sweden) with primers that were either pre-designed or obtained from Bio-Rad Laboratories (Table 1). Quantification cycles (Cq) were determined by CFX Manager Software v3.0 (Bio-Rad Laboratories AB). Absolute quantification was achieved by exponential conversion of the Cq using qPCR efficiency estimated from standard curves obtained by serial dilutions (1/5 dilution) of a pooled sample for each RT set. Relative quantification of the target mRNA was obtained after the normalization with the geometric mean of exponential conversion of the Cq of two reference genes (*Rpl38* and *Hprt*). The geometric mean based on these

genes was similar in both groups. Data were collected with the ABI PRISM 7500 sequence detection system (Applied Biosystems) and analysed using the ΔΔCT method.

Statistics. Statistical analyses were performed with SigmaPlot 13 (Systat Software Inc.). Student's paired, unpaired t tests, one-way ANOVA, or z-test were used as appropriate. Two-way repeated measures ANOVA was used to determine differences between two groups of repeatedly stimulated fibres. The Holm-Sidak post-hoc analysis was used when ANOVA showed a significant difference between groups. Significance was accepted when $P < 0.05$. Data are presented as mean ± SEM.

Acknowledgements

This work was supported by grants from the Swedish Research Council Swedish Research Council (2018-02576), the Swedish Research Council for Sport Science (P2019-0060), Association Française contre les Myopathies (AFM-TELETHON #16798; to C.G.), and the German Research Foundation DFG (FR2993/13-1). For technical support and EM access, we acknowledge the Umeå Centre for Electron Microscopy, the SciLifeLab at Umeå University, the National Microscopy Infrastructure (NMI), including instruments funded by the Knut and Alice Wallenberg foundation and Kempe foundations. Research reported in this publication was supported by the National Institute of Arthritis and Musculoskeletal and Skin Diseases of the National Institutes of Health under award number 1F32AR057619 (NIAMS; to A.H.). The content is solely the responsibility of the authors and does not necessarily represent the official views of the National Institutes of Health.

Conflict of Interests

The laboratory of H.W. received financial support from NeuroVive Pharmaceutical AB (current name: Abliva AB). V.M.L is co-founder and owner of HepaPredict AB.

Author Contributions

C.G., S.U.V., S.Y, A.H., J.D.B., N.I., V.M.L. and H.W. conceived the project and designed the experiments. C.G., S.U.V., S.Y., A.H., A.J.C., T.C., J.D.B. and N.I. performed most of the experiments. A.B., D.S. and O.F. performed Second Harmonic Generation microscopy experiments. K.H. performed TEM experiments. S.H. and L.S. performed FIB-SEM experiments. C.G., S.U.V., N.I., V.M.L. and H.W. wrote the manuscript. All authors contributed to the editing of the manuscript.

References

1. Patti, M.-E., and Corvera, S. (2010). The role of mitochondria in the pathogenesis of type 2 diabetes. Endocr. Rev. *31*, 364-395.
2. Arruda, A.P., and Hotamisligil, G.S. (2015). Calcium homeostasis and organelle function in the pathogenesis of obesity and diabetes. Cell Metab. *22*, 381-397.
3. Zündorf, G., and Reiser, G. (2011). Calcium dysregulation and homeostasis of neural calcium in the molecular mechanisms of neurodegenerative diseases provide multiple targets for neuroprotection. Antioxid. Redox Signal. *14*, 1275-1288.
4. Zhou, B., and Tian, R. (2018). Mitochondrial dysfunction in pathophysiology of heart failure. J. Clin. Invest. *128*, 3716-3726.
5. van der Burgh, R., and Boes, M. (2015). Mitochondria in autoinflammation: cause, mediator or bystander? Trends Endocrinol. Metab. *26*, 263-271.
6. Nakayama, H., and Otsu, K. (2018). Mitochondrial DNA as an inflammatory mediator in cardiovascular diseases. Biochem. J. *475*, 839-852.
7. Giorgi, C., Marchi, S., and Pinton, P. (2018). The machineries, regulation and cellular functions of mitochondrial calcium. Nat. Rev. Mol. Cell Biol. *19*, 713-730.
8. Brookes, P.S., Yoon, Y., Robotham, J.L., Anders, M.W., and Sheu, S.S. (2004). Calcium, ATP, and ROS: a mitochondrial love-hate triangle. Am. J. Physiol. Cell Physiol. *287*, C817-C833.
9. Duchen, M.R. (2000). Mitochondria and Ca^{2+} in cell physiology and pathophysiology. Cell Calcium *28*, 339-348.
10. Rizzuto, R., De Stefani, D., Raffaello, A., and Mammucari, C. (2012). Mitochondria as sensors and regulators of calcium signalling. Nat. Rev. Mol. Cell Biol. *13*, 566-578.
11. Baylor, S.M., and Hollingworth, S. (2007). Simulation of Ca^{2+} movements within the sarcomere of fast-twitch mouse fibers stimulated by action potentials. J. Gen. Physiol. *130*, 283-302.
12. Baughman, J.M., Perocchi, F., Girgis, H.S., Plovanich, M., Belcher-Timme, C.A., Sancak, Y., Bao, X.R., Strittmatter, L., Goldberger, O., Bogorad, R.L., et al. (2011). Integrative genomics identifies MCU as an essential component of the mitochondrial calcium uniporter. Nature *476*, 341-345.
13. De Stefani, D., Raffaello, A., Teardo, E., Szabo, I., and Rizzuto, R. (2011). A forty-kilodalton protein of the inner membrane is the mitochondrial calcium uniporter. Nature *476*, 336-340.
14. Marchi, S., and Pinton, P. (2014). The mitochondrial calcium uniporter complex: molecular components, structure and physiopathological implications. J. Physiol. *592*, 829-839.
15. Pan, X., Liu, J., Nguyen, T., Liu, C., Sun, J., Teng, Y., Fergusson, M.M., Rovira, II, Allen, M., Springer, D.A., et al. (2013). The physiological role of mitochondrial calcium revealed by mice lacking the mitochondrial calcium uniporter. Nat. Cell Biol. *15*, 1464-1472.

16. Kwong, J.Q., Huo, J., Bround, M.J., Boyer, J.G., Schwanekamp, J.A., Ghazal, N., Maxwell, J.T., Jang, Y.C., Khuchua, Z., Shi, K., et al. (2018). The mitochondrial calcium uniporter underlies metabolic fuel preference in skeletal muscle. JCI Insight *3*, e121689.
17. Palty, R., Silverman, W.F., Hershfinkel, M., Caporale, T., Sensi, S.L., Parnis, J., Nolte, C., Fishman, D., Shoshan-Barmatz, V., Herrmann, S., et al. (2010). NCLX is an essential component of mitochondrial Na^+/Ca^{2+} exchange. Proc. Natl. Acad. Sci. U. S. A. *107*, 436-441.
18. Bershadsky, A.D., Balaban, N.Q., and Geiger, B. (2003). Adhesion-dependent cell mechanosensitivity. Annu. Rev. Cell Dev. Biol. *19*, 677-695.
19. Geiger, B., Bershadsky, A., Pankov, R., and Yamada, K.M. (2001). Transmembrane crosstalk between the extracellular matrix--cytoskeleton crosstalk. Nat Rev Mol Cell Biol *2*, 793-805.
20. de Cavanagh, E.M., Ferder, M., Inserra, F., and Ferder, L. (2009). Angiotensin II, mitochondria, cytoskeletal, and extracellular matrix connections: an integrating viewpoint. Amer J Physiol Heart Circ Physiol *296*, H550-H558.
21. Boncompagni, S., Rossi, A.E., Micaroni, M., Beznoussenko, G.V., Polishchuk, R.S., Dirksen, R.T., and Protasi, F. (2009). Mitochondria are linked to calcium stores in striated muscle by developmentally regulated tethering structures. Mol. Biol. Cell *20*, 1058-1067.
22. Ainbinder, A., Boncompagni, S., Protasi, F., and Dirksen, R.T. (2015). Role of Mitofusin-2 in mitochondrial localization and calcium uptake in skeletal muscle. Cell Calcium *57*, 14-24.
23. Tubbs, E., Chanon, S., Robert, M., Bendridi, N., Bidaux, G., Chauvin, M.A., Ji-Cao, J., Durand, C., Gauvrit-Ramette, D., Vidal, H., et al. (2018). Disruption of mitochondria-associated endoplasmic reticulum membrane (MAM) integrity contributes to muscle insulin resistance in mice and humans. Diabetes *67*, 636-650.
24. Kanagawa, M., and Toda, T. (2006). The genetic and molecular basis of muscular dystrophy: roles of cell-matrix linkage in the pathogenesis. J. Hum. Genet. *51*, 915-926.
25. Allen, D.G., Whitehead, N.P., and Froehner, S.C. (2016). Absence of dystrophin disrupts skeletal muscle signaling: Roles of Ca^{2+}, reactive oxygen species, and nitric oxide in the development of muscular dystrophy. Physiol. Rev. *96*, 253-305.
26. Bernardi, P., and Bonaldo, P. (2013). Mitochondrial dysfunction and defective autophagy in the pathogenesis of collagen VI muscular dystrophies. Cold Spring Harb Perspect Biol *5*, a011387.
27. Angelin, A., Tiepolo, T., Sabatelli, P., Grumati, P., Bergamin, N., Golfieri, C., Mattioli, E., Gualandi, F., Ferlini, A., Merlini, L., et al. (2007). Mitochondrial dysfunction in the pathogenesis of Ullrich congenital muscular dystrophy and prospective therapy with cyclosporins. Proc. Natl. Acad. Sci. U. S. A. *104*, 991-996.
28. Merlini, L., Angelin, A., Tiepolo, T., Braghetta, P., Sabatelli, P., Zamparelli, A., Ferlini, A., Maraldi, N.M., Bonaldo, P., and Bernardi, P. (2008). Cyclosporin A corrects mitochondrial

dysfunction and muscle apoptosis in patients with collagen VI myopathies. Proc. Natl. Acad. Sci. U. S. A. *105*, 5225-5229.

29. Irwin, W.A., Bergamin, N., Sabatelli, P., Reggiani, C., Megighian, A., Merlini, L., Braghetta, P., Columbaro, M., Volpin, D., Bressan, G.M., et al. (2003). Mitochondrial dysfunction and apoptosis in myopathic mice with collagen VI deficiency. Nat.Genet. *35*, 367-371.
30. Tiepolo, T., Angelin, A., Palma, E., Sabatelli, P., Merlini, L., Nicolosi, L., Finetti, F., Braghetta, P., Vuagniaux, G., Dumont, J.M., et al. (2009). The cyclophilin inhibitor Debio 025 normalizes mitochondrial function, muscle apoptosis and ultrastructural defects in Col6a1-/- myopathic mice. Br. J. Pharmacol. *157*, 1045-1052.
31. Rossi, A.E., Boncompagni, S., Wei, L., Protasi, F., and Dirksen, R.T. (2011). Differential impact of mitochondrial positioning on mitochondrial Ca^{2+} uptake and Ca^{2+} spark suppression in skeletal muscle. Am. J. Physiol. Cell Physiol. *301*, C1128-C1139.
32. Martins, A.S., Shkryl, V.M., Nowycky, M.C., and Shirokova, N. (2008). Reactive oxygen species contribute to Ca^{2+} signals produced by osmotic stress in mouse skeletal muscle fibres. J.Physiol *586*, 197-210.
33. Wang, X., Weisleder, N., Collet, C., Zhou, J., Chu, Y., Hirata, Y., Zhao, X., Pan, Z., Brotto, M., Cheng, H., et al. (2005). Uncontrolled calcium sparks act as a dystrophic signal for mammalian skeletal muscle. Nat Cell Biol *7*, 525-530.
34. Tarpey, M.D., Amorese, A.J., Balestrieri, N.P., Ryan, T.E., Schmidt, C.A., McClung, J.M., and Spangenburg, E.E. (2018). Characterization and utilization of the flexor digitorum brevis for assessing skeletal muscle function. Skelet Muscle *8*, 14.
35. Marcucci, L., Canato, M., Protasi, F., Stienen, G.J.M., and Reggiani, C. (2018). A 3D diffusional-compartmental model of the calcium dynamics in cytosol, sarcoplasmic reticulum and mitochondria of murine skeletal muscle fibers. PLoS One *13*, e0201050.
36. Cheng, A.J., and Westerblad, H. (2017). Mechanical isolation, and measurement of force and myoplasmic free [Ca^{2+}] in fully intact single skeletal muscle fibers. Nat. Protoc. *12*, 1763-1776.
37. Buttgereit, A., Weber, C., Garbe, C.S., and Friedrich, O. (2013). From chaos to split-ups--SHG microscopy reveals a specific remodelling mechanism in ageing dystrophic muscle. J. Pathol. *229*, 477-485.
38. Garbe, C.S., Buttgereit, A., Schurmann, S., and Friedrich, O. (2012). Automated multiscale morphometry of muscle disease from second harmonic generation microscopy using tensor-based image processing. IEEE Trans. Biomed. Eng. *59*, 39-44.
39. Murphy, G.E., Lowekamp, B.C., Zerfas, P.M., Chandler, R.J., Narasimha, R., Venditti, C.P., and Subramaniam, S. (2010). Ion-abrasion scanning electron microscopy reveals distorted liver mitochondrial morphology in murine methylmalonic acidemia. J. Struct. Biol. *171*, 125-132.

40. Friedmann, A., Cismak, A., Tautorat, C., Koester, P.J., Baumann, W., Held, J., Gaspar, J., Ruther, P., Paul, O., and Heilmann, A. (2012). FIB preparation and SEM investigations for three-dimensional analysis of cell cultures on microneedle arrays. Scanning *34*, 221-229.

41. Aydin, J., Andersson, D.C., Hänninen, S.L., Wredenberg, A., Tavi, P., Park, C.B., Larsson, N.G., Bruton, J.D., and Westerblad, H. (2009). Increased mitochondrial Ca^{2+} and decreased sarcoplasmic reticulum Ca^{2+} in mitochondrial myopathy. Hum. Mol. Genet. *18*, 278-288.

42. Matlib, M.A., Zhou, Z., Knight, S., Ahmed, S., Choi, K.M., Krause-Bauer, J., Phillips, R., Altschuld, R., Katsube, Y., Sperelakis, N., et al. (1998). Oxygen-bridged dinuclear ruthenium amine complex specifically inhibits Ca^{2+} uptake into mitochondria in vitro and in situ in single cardiac myocytes. J. Biol. Chem. *273*, 10223-10231.

43. Griffiths, E.J. (2009). Mitochondrial calcium transport in the heart: physiological and pathological roles. J. Mol. Cell. Cardiol. *46*, 789-803.

44. Azzi, J.R., Sayegh, M.H., and Mallat, S.G. (2013). Calcineurin inhibitors: 40 years later, can't live without. J. Immunol. *191*, 5785-5791.

45. Connern, C.P., and Halestrap, A.P. (1992). Purification and N-terminal sequencing of peptidyl-prolyl cis-trans-isomerase from rat liver mitochondrial matrix reveals the existence of a distinct mitochondrial cyclophilin. Biochem. J. *284* 381-385.

46. Giorgio, V., Soriano, M.E., Basso, E., Bisetto, E., Lippe, G., Forte, M.A., and Bernardi, P. (2010). Cyclophilin D in mitochondrial pathophysiology. Biochim. Biophys. Acta *1797*, 1113-1118.

47. Halestrap, A.P., and Davidson, A.M. (1990). Inhibition of Ca^{2+}-induced large-amplitude swelling of liver and heart mitochondria by cyclosporin is probably caused by the inhibitor binding to mitochondrial-matrix peptidyl-prolyl *cis-trans* isomerase and preventing it interacting with the adenine nucleotide translocase. Biochem. J. *268*, 153-160.

48. Crompton, M., Ellinger, H., and Costi, A. (1988). Inhibition by cyclosporin A of a Ca^{2+}-dependent pore in heart mitochondria activated by inorganic phosphate and oxidative stress. Biochem. J. *255*, 357-360.

49. Broekemeier, K.M., Dempsey, M.E., and Pfeiffer, D.R. (1989). Cyclosporin A is a potent inhibitor of the inner membrane permeability transition in liver mitochondria. J. Biol. Chem. *264*, 7826-7830.

50. Baines, C.P., and Gutierrez-Aguilar, M. (2018). The still uncertain identity of the channel-forming unit(s) of the mitochondrial permeability transition pore. Cell Calcium *73*, 121-130.

51. Gineste, C., Hernandez, A., Ivarsson, N., Cheng, A.J., Naess, K., Wibom, R., Lesko, N., Bruhn, H., Wedell, A., Freyer, C., et al. (2015). Cyclophilin D, a target for counteracting skeletal muscle dysfunction in mitochondrial myopathy. Hum. Mol. Genet. *24*, 6580-6587.

52. Seidlmayer, L.K., Juettner, V.V., Kettlewell, S., Pavlov, E.V., Blatter, L.A., and Dedkova, E.N. (2015). Distinct mPTP activation mechanisms in ischaemia-reperfusion: contributions of Ca^{2+}, ROS, pH, and inorganic polyphosphate. Cardiovasc. Res. *106*, 237-248.
53. Hansson, M.J., Moss, S.J., Bobardt, M., Chatterji, U., Coates, N., Garcia-Rivera, J.A., Elmer, E., Kendrew, S., Leyssen, P., Neyts, J., et al. (2015). Bioengineering and semisynthesis of an optimized cyclophilin inhibitor for treatment of chronic viral infection. Chem. Biol. *22*, 285-292.
54. Wredenberg, A., Wibom, R., Wilhelmsson, H., Graff, C., Wiener, H.H., Burden, S.J., Oldfors, A., Westerblad, H., and Larsson, N.G. (2002). Increased mitochondrial mass in mitochondrial myopathy mice. Proc. Natl. Acad. Sci. U. S. A. *99*, 15066-15071.
55. Lagouge, M., Mourier, A., Lee, H.J., Spahr, H., Wai, T., Kukat, C., Silva Ramos, E., Motori, E., Busch, J.D., Siira, S., et al. (2015). SLIRP regulates the rate of mitochondrial protein synthesis and protects LRPPRC from degradation. PLoS Genet *11*, e1005423.
56. Allen, D.G., and Westerblad, H. (1995). The effects of caffeine on intracellular calcium, force and the rate of relaxation of mouse skeletal muscle. J. Physiol. *487*, 331-342.
57. Duval, K., Grover, H., Han, L.H., Mou, Y., Pegoraro, A.F., Fredberg, J., and Chen, Z. (2017). Modeling physiological events in 2D vs. 3D cell culture. Physiology (Bethesda) *32*, 266-277.
58. Liao, H., Qi, Y., Ye, Y., Yue, P., Zhang, D., and Li, Y. (2020). Mechanotranduction pathways in the regulation of mitochondrial homeostasis in cardiomyocytes. Front Cell Dev Biol *8*, 625089.
59. Bartolák-Suki, E., Imsirovic, J., Nishibori, Y., Krishnan, R., and Suki, B. (2017). Regulation of mitochondrial structure and dynamics by the cytoskeleton and mechanical factors. Int. J. Mol. Sci. *18*, 1812.
60. Lackner, L.L. (2014). Shaping the dynamic mitochondrial network. BMC Biol *12*, 35.
61. Machado, L., Esteves de Lima, J., Fabre, O., Proux, C., Legendre, R., Szegedi, A., Varet, H., Ingerslev, L.R., Barrès, R., Relaix, F., et al. (2017). In situ fixation redefines quiescence and early activation of skeletal muscle stem cells. Cell Rep *21*, 1982-1993.
62. van Velthoven, C.T.J., de Morree, A., Egner, I.M., Brett, J.O., and Rando, T.A. (2017). Transcriptional profiling of quiescent muscle stem cells *in vivo*. Cell rep. *21*, 1994-2004.
63. McAdam, M.E., Levelle, F., Fox, R.A., and Fielden, E.M. (1977). A pulse-radiolysis study of the manganese-containing superoxide dismutase from Bacillus stearothermophilus. Biochem. J. *165*, 81-87.
64. Hearn, A.S., Tu, C., Nick, H.S., and Silverman, D.N. (1999). Characterization of the product-inhibited complex in catalysis by human manganese superoxide dismutase. J. Biol. Chem. *274*, 24457-24460.

65. Plotnikov, S.V., Millard, A.C., Campagnola, P.J., and Mohler, W.A. (2006). Characterization of the myosin-based source for second-harmonic generation from muscle sarcomeres. Biophys. J. *90*, 693-703.

66. Schneidereit, D., Nübler, S., Prölss, G., Reischl, B., Schürmann, S., Müller, O.J., and Friedrich, O. (2018). Optical prediction of single muscle fiber force production using a combined biomechatronics and second harmonic generation imaging approach. Light Sci. Appl. *7*, 79.

67. Deerinck, T.J., Bushong, E., Thor, A., and Ellisman, M. (2010). NCMIR methods for 3D EM: A new protocol for preparation of biological specimens for serial block face scanning electron microscopy. Nat Center Microsc Imag Res, 6-8.

68. Kremer, J.R., Mastronarde, D.N., and McIntosh, J.R. (1996). Computer visualization of three-dimensional image data using IMOD. J. Struct. Biol. *116*, 71-76.

Table 1: Primers used for expression profiling of transcripts in skeletal muscle.

***Gene* (protein)**		**Sequence/Assay ID**
Rpl38 (ribosomal protein L38)	Forward Reverse	GGTTCTCATCGCTGTGAGTGT AATTTTCCGAGGCATGGCGA
Hprt (hypoxanthine-guanine phosphoribosyl transferase)	Forward Reverse	ACAGGCCAGACTTTGTTGGA ACTTGCGCTCATCTTAGGCT
Col6a1 (collagen 6)		qMmuCID0015430
Des (desmin)		qMmuCID0005564
Dmd (dystrophin)		qMmuCID0018306
Lamb2 (laminin 2)		qMmuCED0049837
Ttn (titin)		qMmuCED0037550